MOLECULAR ONCOLOGY 8 (2014) 1240–1252

available at www.sciencedirect.com

ScienceDirect

www.elsevier.com/locate/molonc

Expression patterns of bone morphogenetic protein antagonists in colorectal cancer desmoplastic invasion fronts

George S. Karagiannis[a,b], Ann Treacy[c], David Messenger[d,e], Andrea Grin[a,f], Richard Kirsch[a,b], Robert H. Riddell[a,b], Eleftherios P. Diamandis[a,b,g,*]

[a]Department of Laboratory Medicine and Pathobiology, University of Toronto, Toronto, Ontario, Canada
[b]Department of Pathology and Laboratory Medicine, Mount Sinai Hospital, Toronto, Ontario, Canada
[c]MC Pathology, The Laboratory, Charlemont Clinic, Charlemont Mall, Dublin, Ireland
[d]Zane Cohen Clinical Research Centre, Mount Sinai Hospital, Toronto, Canada
[e]Division of General Surgery, Mount Sinai Hospital, Toronto, Canada
[f]Department of Laboratory Medicine, St Michael's Hospital, Toronto, Canada
[g]Department of Clinical Biochemistry, University Health Network, Toronto, Ontario, Canada

ARTICLE INFO

Article history:
Received 9 February 2014
Received in revised form
24 February 2014
Accepted 9 April 2014
Available online 19 April 2014

Keywords:
Bone morphogenetic protein antagonists
Gremlin-1
Follistatin
High-temperature requirement-A3
Tumor budding
Cancer-associated fibroblasts
Colorectal cancer

ABSTRACT

Bone morphogenetic proteins (BMPs) are a group of growth factors with dual functions in cancer development and progression. Recently, certain tumor-promoting roles have been identified for selected antagonists/inhibitors (BMPIs) of this developmental pathway. A recent focus on the implication of BMP in colorectal cancer progression has emerged, mainly due to the presence of inactivating mutations in several members of the canonical signaling cascade. However, the detailed expression profiles of BMPIs remain largely unknown. Based on our previous work, whereby three specific BMPIs, gremlin-1 (GREM1), high-temperature requirement A3 (HTRA3) and follistatin (FST) were collectively overexpressed in desmoplastic cocultures of colorectal cancer (CRC), here, we undertook an immunohistochemical approach to describe the patterns of their expression in CRC patients. Two major characteristics described the BMPI expression signature: First, the synchronous and coordinated stromal and epithelial overexpression of individual BMPIs in desmoplastic lesions, which demonstrated that all three of them contribute to increasing levels of BMP antagonism in such areas. Second, the presence of microenvironmental polarity in the BMPI pattern of expression, which was indicated through the preferential expression of HTRA3 in the stromal, and the parallel FST/GREM1 expression in the epithelial component of the investigated sections. In addition, expression of HTRA3 in the epithelial compartment of the tumors demonstrated a significant predictive power to

Abbreviations: AUC, area under the curve; BMP(I), bone morphogenetic protein (inhibitor); h-CALD, h-caldesmon; β-CAT, β-catenin; EMT, epithelial-to-mesenchymal transition; FST, follistatin; GREM1, gremlin-1; HGTB, high-grade tumor-budding; HL, Hosmer–Lemeshow; HTRA3, high temperature requirement A3; IHC, immunohistochemistry; LAMB1, laminin-β1; LGTB, low-grade tumor-budding; MSI, microsatellite instability; NTB, no tumor-budding; ROC, receiver operating characteristic; α-SMA, α-smooth muscle actin; TBS, tumor-budding score; TGF-β, transforming growth factor-β; TIL, tumor-infiltrating lymphocyte; VEGFR2, vascular endothelial growth factor receptor-2.

* *Corresponding author*. Mount Sinai Hospital, Joseph & Wolf Lebovic Ctr., 60 Murray St. [Box 32], Floor 6 – Room L6-201, Toronto, ON, M5T 3L9 Canada. Tel.: +1 416 586 8443; fax: +1 416 619 5521.
E-mail address: ediamandis@mtsinai.on.ca (E.P. Diamandis).

http://dx.doi.org/10.1016/j.molonc.2014.04.004

discriminate between tumor-budding-bearing and tumor-budding-free desmoplastic microenvironments. Together, these findings contribute to the understanding of signaling dynamics of BMP antagonism in the colorectal cancer desmoplastic invasion front.

1. Introduction

Bone morphogenetic proteins (BMPs) are a group of growth factors, also known as cytokines, originally discovered by their ability to regulate formation of bone and cartilage, but currently demonstrated to exert a wide range of morphogenetic activity that is both tissue- and context-dependent (Reddi and Reddi, 2009). Cancer often involves dysregulation of the BMP signaling pathway (Singh and Morris, 2010). However, the precise role of BMPs in cancer remains rather elusive. On one hand, there are well-established tumor-promoting effects linking BMPs, their receptors and interacting molecules to carcinogenesis and tumor progression, but BMPs can sometimes play the role of tumor suppressors (Singh and Morris, 2010).

Among the multitude of suppressive roles, it has been demonstrated that the BMP pathway promotes the sustenance of the epithelial phenotype in various cell types and cell lineages (Zeisberg et al., 2003), as well as in breast and colorectal cancer (CRC) (Alarmo and Kallioniemi, 2010; Beck et al., 2006). Recent data suggest that sporadic CRC may disrupt the tumor-suppressive effects of BMP signaling through genomic mutations of SMAD4 and BMP receptor type II (Kodach et al., 2008; Kotzsch et al., 2008). Epigenetic mechanisms for disruption of the suppressive BMP signaling in gastrointestinal tract tumors have also been suggested (Wen et al., 2006). We (Karagiannis et al., 2013a) and others (Sneddon et al., 2006) have additionally demonstrated that the expression of BMP antagonists/inhibitors (BMPIs), such as gremlin-1, may impair BMP2/7 signaling and promote tumor cell motility and proliferation.

Earlier studies in our laboratory on SW480 and SW620 cocultures with primary normal colonic fibroblasts identified three BMPIs, namely gremlin-1 (GREM1), follistatin (FST) and high-temperature requirement A3 (HTRA3), which also regulate other pathways in the transforming growth factor-β (TGF-β) superfamily of proteins (Karagiannis et al., 2012a). Specifically, all three BMPIs were abundantly expressed in desmoplastic cocultures, but were not secreted by control monocultures. Accumulating evidence from our (Karagiannis et al., 2012b; 2013a) and other groups (Namkoong et al., 2006; Sneddon, 2009; Sneddon et al., 2006) suggest that GREM1 may be microenvironmentally regulated and expressed by both cancer-associated fibroblasts (CAFs) and cancer cells in the invasive margins in a variety of desmoplastic cancers. However, the exact pattern of BMPI expression is largely unknown in the tumor-host cell interface, especially in the CRC desmoplastic microenvironment.

Here, we undertook an immunohistochemical (IHC) approach to describe the expression of these BMPIs in two independent cohorts of patients with invasive CRC. We assessed both stromal and epithelial expression of these BMPIs in desmoplastic invasion fronts and characterized the independent contribution of each BMPI determinant in the overall BMPI expression signature.

2. Materials and methods

2.1. Patient cohorts

The study involved two distinct patient cohorts, both randomly obtained from a larger well-established cohort of 219 patients with invasive CRC (Supplementary Table 1), first described in our previous study (Grin et al., 2013). The discovery (hypothesis-generating) cohort ($n = 30$) was blindly selected with respect to creating three independent groups based on histological criteria defining the tumor-budding population, as previously described (Mitrovic et al., 2012). In particular, high-grade tumor-budding ($n = 10$), low-grade tumor-budding ($n = 10$) and tumor-budding-free ($n = 10$) patient groups were selected.

The REMARK guidelines and principles were followed for the design of the verification study (Altman et al., 2012). The validation (hypothesis-verifying) cohort ($n = 38$) had the following clinicopathologic characteristics: (1) median follow-up of survivors: 56 months (range 0–79; interquartile range 14–64); (2) median age of cohort: 67.5 years (range 34–89; interquartile range 60–77); (3) percentage of males: 55.3% ($n = 21$); (4) disease location: of the 20 right sided cancers (52.6%), 11 (28.9%) were located in the caecum, 6 (15.8%) in the ascending colon and 2 (5.3%) in the transverse colon and 1 (2.6%) in the splenic flexure. Of the 18 left-sided cancers (47.4%), 2 (5.3%) were located in the descending colon, 12 (31.6%) in the sigmoid colon and 4 (10.6%) at the recto-sigmoid junction/upper rectum; (5) 30-day mortality: 5.3% ($n = 2$); (6) T-Category: 30 (78.9%) were classified as pT3 and 8 (21.1%) as pT4; (7) the 5-year disease-free survival (DFS) was 68.1% and the 5-year overall survival (OS) was 81.6%; (8) Regarding tumor-budding, 14 cases (36.8%) were identified with medium/high tumor-budding (TB > or = 5); (9) Crohn's like reaction was present in 5 cases (13.1%); (10) marked tumor-infiltrating lymphocytes (marked-TILs) were found in 7 cases (18.5%).

2.2. Immunohistochemistry (IHC)

Staining was carried out as previously described (Karagiannis et al., 2014). The following primary antibodies were used: α-smooth muscle actin (α-SMA; Clone 1A4, dilution 1:200, Dako), h-caldesmon (h-CALD; dilution 1:400; Dako), laminin-beta1, (LAMB1; rabbit polyclonal; dilution 1:400; Sigma), beta-

catenin (β-CAT; clone 14; 1:200; BDBioscience), as well as the three BMP inhibitors GREM1 (rabbit polyclonal; dilution 1:200; Abcam), HTRA3 (rabbit polyclonal; dilution 1:300; Sigma) and FST (rabbit polyclonal; dilution 1:50; Sigma).

2.3. Immunohistochemical scoring

2.3.1. Area selection

Based on the concept of "tumor development along with the surrounding context", described by the Mina Bissell group (Bissell and Radisky, 2001), as well as our previous work on CRC desmoplasia (Karagiannis et al., 2012a), here, we assumed that the expression of BMP antagonists GREM1, HTRA3 and FST is restricted in specialized microenvironments, such as the desmoplastic invasion front. A small number (n = 1–6) of sections in each specimen, encompassing such microenvironments, was randomly selected in each case, based on β-CAT staining, which provides adequate discriminatory power between cancer and stromal cell populations (Supplementary Figure 1). Areas encompassing tissue lifting or limited tissue on the slides, edge artifacts, high background staining and abundant mucinous component were excluded. The desmoplastic nature of the acquired areas was verified with the myofibroblastic markers α-smooth muscle actin (α-SMA) and laminin-β1 (LAMB1), as well as the smooth-muscle marker h-caldesmon (CALD). Only peritumoral stromata, bearing an expression signature reminiscent of the desmoplastic microenvironment (i.e. α-SMA positive, LAMB1 positive, h-CALD negative or focally-positive) was accepted for further consideration in this study (Supplementary Figure 2). Overall, 90 and 167 areas fulfilled these quality control criteria for the discovery and validation cohorts, respectively.

2.3.2. Scoring of the BMPIs

Of the 90 areas selected in the discovery cohort, a total of 35 had tumor-budding populations and were named as: "tumor-budding areas", while 55 did not have tumor-budding, and were termed as "invasion fronts" (Table 1). Using histological criteria proposed from our group (Mitrovic et al., 2012), the areas were also classified according to their tumor-budding score (TBS) into: "no tumor-budding" (NTB; 0 < TBS < 5; n = 55), "low-grade tumor-budding" (LGTB; 5.1 < TBS < 10; n = 18) and "high-grade tumor-budding (HGTB; 10.1 < TBS < 15; n = 17) (Table 1). GREM1, HTRA3 and FST were scored for both epithelial (e) and stromal (s) compartment of the tumors in all 90 areas, either these simply represented invasion fronts or tumor-budding areas. Therefore, the following independent scores were obtained: eGREM1, sGREM1, eHTRA3, sHTRA3, eFST and sFST, here termed as "BMPI determinants". To obtain a single numerical value for each of these determinants, two independent parameters were co-assessed: the staining intensity (SI) and the staining percentage (SP). For the BMPI determinant under investigation, the SI was scored with 0 (no intensity), 1 (low intensity), and 2 (strong intensity) (Supplementary Figure 3). Accordingly, the SP was scored with 0 (0% of area is positive), 1 (0.1–10% of area is positive), 2 (10.1–50% of area is positive), and 3 (50.1–100% of area is positive). The two parameters were multiplied to provide the final score for each BMPI determinant in each area [e.g. eGREM1 = (SI)eGREM1*(SP)eGREM1]. From the range of the numerical values of the SI and SP parameters, it follows that each determinant could be designated with a score of 0–6.

Total scores for GREM1 (tGREM1), HTRA3 (tHTRA3) and FST (tFST), were calculated by combining the individual scores for (e) and (s) BMPI determinants [e.g. tGREM1 = eGREM1+ sGREM1]. Thus, each of the tGREM1, tHTRA3 and tFST values could be designated with a score of 0–12. Finally, for each area, the total BMPI (tBMPI) index was calculated from scores of all three BMPIs [tBMPI = tGREM1 + tHTRA3 + tFST]. Thus, tBMPI obtained a numerical value of 0–36 in each area. Based on the tBMPI scores, we classified the areas into Q1 (n = 22; tBMPI = 0–3; low BMPI-expressing quartile), Q2 (n = 26; tBMPI = 4–7; low-medium BMPI-expressing quartile), Q3 (n = 21; tBMPI = 8–11; medium–high BMPI-expressing quartile) and Q4 (n = 21; tBMPI = 11–36; high BMPI-expressing quartile). Each one of these quartiles represents 25% of the

Table 1 – Classifications of the selected areas of the discovery cohort (N = 90).

	Frequency (N)	Percent (%)	Cum. percent (%)
Nature of areas[a]			
Invasive fronts	55	61.1	61.1
Tumor-budding areas	35	38.9	100
Tumor-budding grade[b]			
NTB[c]	55	61.1	61.1
LGTB[c]	18	20	81.1
HGTB[c]	17	18.9	100
tBMPI expression score quartiles[d]			
Q1 (tBMPI = 0–3; Mean = 1.73)	22	24.4	24.4
Q2 (tBMPI = 4–7; Mean = 5.65)	26	28.8	53.2
Q3 (tBMPI = 8–11; Mean = 9.24)	21	23.4	76.6
Q4 (tBMPI = 11–26; Mean = 16.95)	21	23.4	100

a Type of area defined by β-CAT staining (refer to: Materials & Methods).
b Grade defined based on the histological criteria proposed by Mitrovic et al. (2012) (refer to: Materials & Methods).
c Abbreviations: NTB, no tumor-budding; LGTB, low-grade tumor-budding; HGTB, high-grade tumor-budding.
d Classification of areas into quartiles based on the area's tBMPI expression score (refer to: Materials & Methods).

total 90 selected areas (Table 1). It follows that this classification may categorize the areas into varying levels/degrees of BMP antagonism, regardless of which individual BMPIs contribute to the overall antagonism.

Of the 167 areas selected in the validation cohort, a total of 89 belonged to invasion fronts with presence of tumor budding, while the remainder 78 was invasion fronts free of tumor-budding population. This cohort was used for verifying the difference in the expression of eHTRA3 between these two types of areas.

2.3.3. *Quality controls*

Bone morphogenetic protein antagonists have been shown to be expressed by naturally-occurring myofibroblasts around healthy colonic crypts, whereby they support the stem-cell niche and the differentiation gradient of the normal colonic epithelium along the crypt axis (Karagiannis et al., 2012b; Saaf et al., 2007). As such, pericryptal expression of GREM1, HTRA3 and FST served as positive internal controls. Negative controls were performed by omitting the primary antibody step, and by evaluating in-built negative controls in each specimen separately (e.g. muscularis propria, inflammatory cells and endothelial cells). A few examples are shown in Supplementary Figure 4. Areas not following quality control criteria described above were removed from the study.

2.4. *Statistical analysis*

The SPSS (version 20) software was used for all analyses. Data regarding expression levels of various BMPIs were presented as bars of means with their standard error. BMPI signature patterns were shown as lines indicating means with their standard error.

The Kolmogorov–Smirnov statistic was performed to test for normality of distribution in the BMPI score values. In cases where data did not follow a normal distribution, the non-parametric Mann–Whitney *U*-test was utilized to compare BMPI scores between two independent groups of areas. In cases where data followed a normal distribution, the parametric independent-samples student's *t*-test was utilized instead. In these cases, the Levene's test was *a priori* performed to test for equality of variances between the two groups. Whenever equal variances could not be assumed, the Levene's correction in degrees of freedom was performed for correcting the obtained *p*-values. The non-parametric Wilcoxon test was used to compare BMPI scores between two matched/paired area groups. Where applicable, line diagrams demonstrating the ratio of expressions for individual BMPIs between (*e*) and (s) compartments (i.e. "microenvironmental polarity" diagrams) were constructed. In these cases, the angles of inclination were tested for statistically significant difference from an angle of inclination equal to "0", using the non-parametric chi-square statistic. The non-parametric Jonckheere–Terpstra test was used for comparing individual BMPI scores among multiple independent area groups. For correlations, the non-parametric Spearman's ranked correlation coefficient was applied. Correlation matrices for multiple variables were created using Spearman's rho values. Statistical significance was shown at either 0.05 or 0.01 level.

For logistic regression analysis, prediction criterion was a dichotomous variable either designated as "tumor-budding areas" ($N = 35$) or "invasion fronts" ($N = 55$). Factor included in the analysis was the epithelial expression of the BMP antagonist HTRA3 (i.e. eHTRA3). A p-value < 0.05 was regarded as statistically significant. Goodness-of-fit was *a priori* performed with the Hosmer–Lemeshow (HL) statistic; p-value < 0.05 was considered significant to show improper data calibration. Receiver operating characteristic (ROC) curves were used to assess the adequacy of the predictive power. Cross-tabulation was used to assess sensitivity and specificity. For validation purposes, the logistic regression model was performed using eHTRA3 expression scores from the validation cohort. In the latter case, a series of co-factors such as gender, T-category, Lymph node yield, status of intravascular invasion, presence of Crohn's like lesions and marked tumor-infiltrating lymphocytes (marked-TILs) were additionally included in the classification model.

Table 2 – Descriptive statistics from scoring of three bone morphogenetic protein inhibitors in areas ($N = 90$) of 30 patients with invasive colorectal cancer.

BMPIs[a]	Minimum	Maximum	Mean	Std. error	Std. dev	Variance
eGREM1	0	6	1.61	0.18	1.707	2.914
sGREM1	0	6	0.84	0.138	1.306	1.706
tGREM1[b]	0	10	2.46	0.284	2.691	7.24
eHTRA3	0	6	1.01	0.16	1.518	2.303
sHTRA3	0	6	2.36	0.162	1.538	2.367
tHTRA3[b]	0	12	3.37	0.27	2.564	6.572
eFST	0	6	1.77	0.153	1.454	2.113
sFST	0	3	0.58	0.087	0.821	0.674
tFST[b]	0	7	2.35	0.193	1.831	3.352
tBMPI[c]	0	26	8.17	0.626	5.935	35.219

a BMPI, bone morphogenetic protein inhibitor; GREM1, gremlin 1, HTRA3, high-temperature requirement A3; FST, follistatin.
b Total expression was calculated by combining the s and e values of each individual BMPI (refer to: Materials & Methods).
c Total BMP antagonism was calculated by combining the t values of all BMPIs (refer to: Materials & Methods).

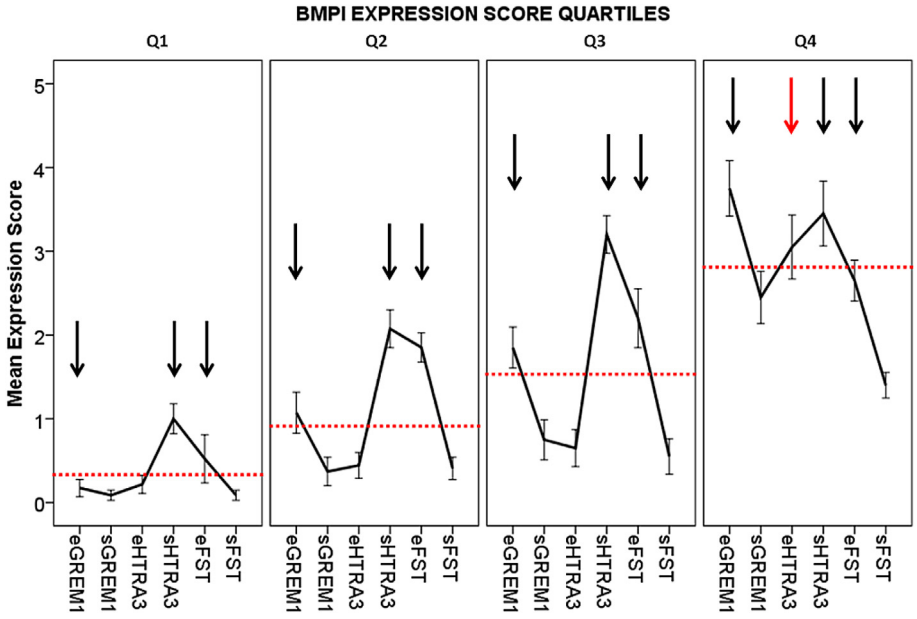

Figure 1 – Pattern of BMPI expression across four quartiles of increasing BMP antagonism. Values are shown as mean expression scores with standard errors. Red-dashed lines: mean expression score of tBMPI in the corresponding quartile; black arrows: peaks corresponding to the conserved eGREM1, sHTRA3 and sFST determinants; red arrow: newly-appearing peak in the Q4 quartile corresponding to the eHTRA3 determinant.

3. Results

3.1. *BMPI expression in colorectal cancer desmoplastic invasion fronts*

In each of the 90 selected areas in the discovery cohort, six independent scores corresponding to either stromal (*s*) or epithelial (*e*) expression of GREM1, HTRA3 and FST, were provided. Descriptive statistics for eGREM1, sGREM1, eHTRA3, sHTRA3, eFST and sFST, here termed as "BMPI determinants", are shown in Table 2. Interestingly, all BMPIs were expressed in both epithelial and stromal compartments of CRC desmoplastic invasion fronts. The highest mean expression score was noticed for HTRA3 (tHTRA3; mean, 3.37; standard error, 0.27), followed by GREM1 (tGREM1; mean, 2.46; standard error, 0.284) and FST (tFST; mean, 2.35; standard error, 0.193). Total BMPI values (tBMPI; mean, 8.17; standard error, 0.626) (Table 2) defined 4 quartiles (Q1–Q4) of areas, corresponding to increasing levels of BMP antagonism (Table 1).

3.2. *Coordinated epithelial and stromal expression of BMPIs in desmoplastic invasion fronts*

In a first attempt to characterize the BMPI expression signature in CRC, we investigated the expression pattern of six BMPI determinants across increasing levels of BMP antagonism. The signature tended to retain a similar pattern of BMPI expression from low- to high-BMPI-expressing quartiles of selected areas (Figure 1; dashed red lines demonstrate the mean tBMPI in each quartile). Moreover, it was clear that all six BMPI determinants could contribute to some extent in the increasing levels of BMP antagonism (Figure 1).

We validated this observation using two independent statistical methods. First, by comparing the expression of the six BMPI determinants among the Q1–Q4 areas, we found statistically significant differences ($p < 0.01$; Jonckheere–Terpstra test) in the ranked expression scores for all six of them (Figure 2A). All BMPI determinants exhibited stable increase in their mean expression scores across the Q1–Q4 areas (Figure 2A). Also, although Q1 areas were almost deficient in eGREM1expression, this BMPI determinant presented with the highest mean expression score among all investigated BMPI determinants in the areas of high BMP antagonism (i.e. Q4 areas) (Figure 2A).

Second, by correlating the total expression scores of the three BMPIs, we found statistically significant associations ($p < 0.01$; Spearman's ranked correlation coefficient) between all combinations of correlations (i.e. tGREM1/tHTRA3, tGREM1/tFST and tHTRA3/tFST) (Figure 2B). In addition, when we performed correlation studies using the individual (s) and (e) scores, we again came across statistically significant associations ($p < 0.01$ or $p < 0.05$, refer to Figure 2C for details; Spearman's ranked correlation coefficient) between all possible combinations of correlations (with the exception of certain correlations regarding the eHTRA3 determinant). As illustrated from the respective correlation matrices (Figure 2B–C), the calculated correlations were all positive (Spearman's rho > 0), signifying coordinated increase of mean expression score values for all BMPIs.

Two representative areas, the first (tGREM1 = 0; tHTRA3 = 2; tFST = 0, tBMPI = 2) derived from Q1 quartile, while the second (tGREM1 = 10; tHTRA3 = 7; tFST = 5; tBMPI = 22) derived from Q4 quartile are shown (Figure 2D). Together, they illustrate differences in the immunoreactivity of BMPI determinants in areas with varying levels of BMP antagonism.

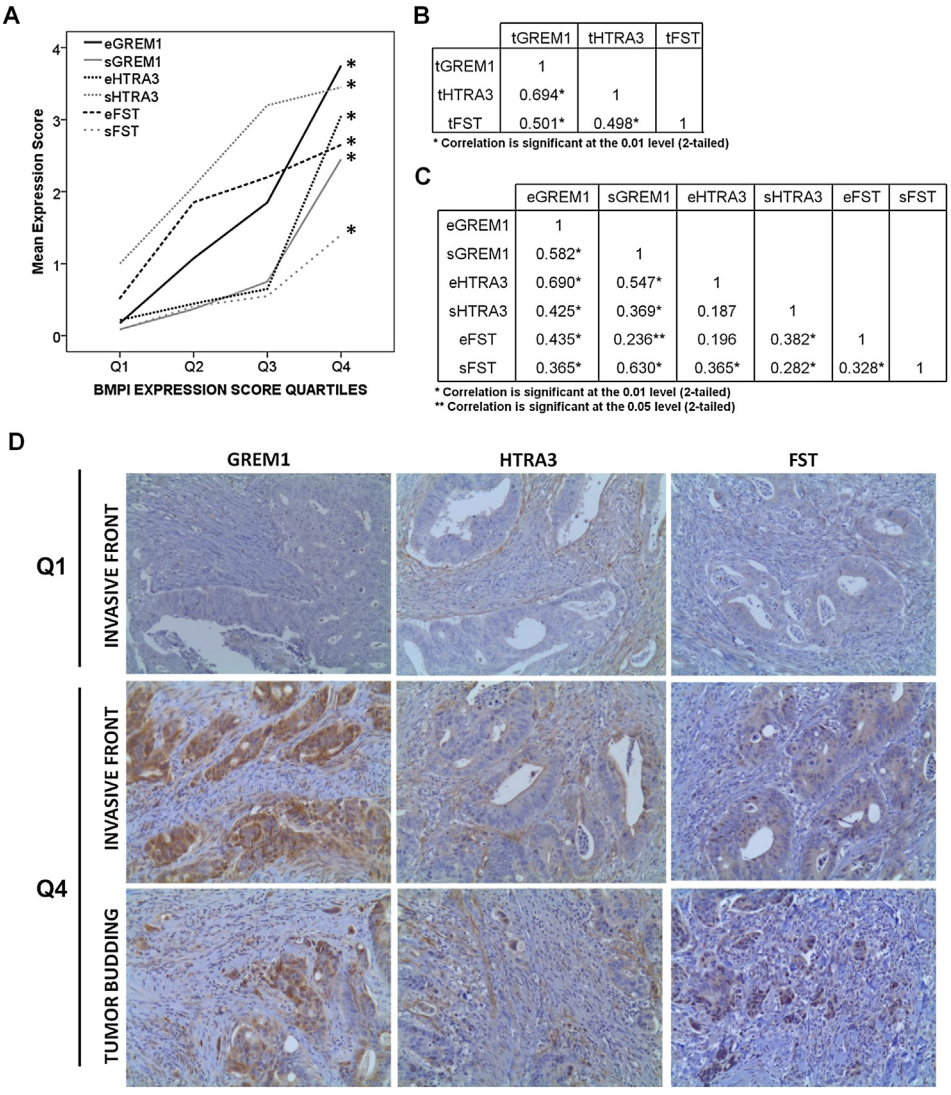

B

	tGREM1	tHTRA3	tFST
tGREM1	1		
tHTRA3	0.694*	1	
tFST	0.501*	0.498*	1

* Correlation is significant at the 0.01 level (2-tailed)

C

	eGREM1	sGREM1	eHTRA3	sHTRA3	eFST	sFST
eGREM1	1					
sGREM1	0.582*	1				
eHTRA3	0.690*	0.547*	1			
sHTRA3	0.425*	0.369*	0.187	1		
eFST	0.435*	0.236**	0.196	0.382*	1	
sFST	0.365*	0.630*	0.365*	0.282*	0.328*	1

* Correlation is significant at the 0.01 level (2-tailed)
** Correlation is significant at the 0.05 level (2-tailed)

Figure 2 – Coordinated epithelial and stromal expression of multiple BMPIs in colorectal cancer desmoplastic invasion fronts. (A) Patterns of mean expression scores of BMPI determinants across Q1–Q4 quartiles. Asterisks demonstrate statistically significant changes across the four groups with Jonckheere–Terpstra test ($p < 0.01$) (B–C) Correlation matrices for all possible combinations of total expression scores of three BMPIs (B) or individual (s) and (e) expression scores for all three BMPIs (C). The numbers indicate Spearman's rho for each combination. Asterisks demonstrate significance in either 0.05 level (**) or 0.01 level (*) with Spearman's ranked correlation coefficient. (D) IHC snapshots from three selected areas, demonstrating the combined expression of BMPIs with increasing levels of overall BMP antagonism. Magnifications ×200.

3.3. *Microenvironmental polarity of BMPI expression in desmoplastic invasion fronts*

The observed 'peaks' on the BMPI expression pattern across Q1–Q4 groups almost conservatively corresponded to three particular BMPI determinants, namely the eGREM1, sHTRA3 and eFST ones (Figure 1; black arrows). This led us to hypothesize that the repertoire of BMPIs participating in BMP antagonism is polarized, i.e. it is different but consistent for each BMPI on both sides of the tumor-host cell interface. The highest mean expression score in the stromal BMPI determinants was noticed for sHTRA3 (mean, 2.36; standard error, 0.162), followed by sGREM1 (mean, 0.84; standard error, 0.138) and sFST (mean, 0.58; standard error, 0.087) (Table 2). Also, the highest mean expression score in the epithelial BMPI determinants was noticed for eFST (mean, 1.77; standard error, 0.153), followed by eGREM1 (mean, 1.61; standard error, 0.18) and eHTRA3 (mean, 1.01; standard error, 0.16) (Table 2). Accordingly, both GREM1 and FST demonstrated a preferential expression in the epithelial compartments ($p < 0.05$; Wilcoxon test), while HTRA3 in the respective stromal compartments of the tumors investigated ($p < 0.05$; Wilcoxon test), regardless of area type (i.e. invasion front or tumor-budding area) (Figure 3A–C, Table 2).

Microenvironmental polarity of GREM1/FST expression in the epithelial compartment was also demonstrated through significantly higher mean expression scores of both eGREM1 and eFST compared to eHTRA3 ($p < 0.05$; Wilcoxon test), across increasing BMPI-expression score quartiles (Figure 3D). An exception to this observation was the Q4 areas,

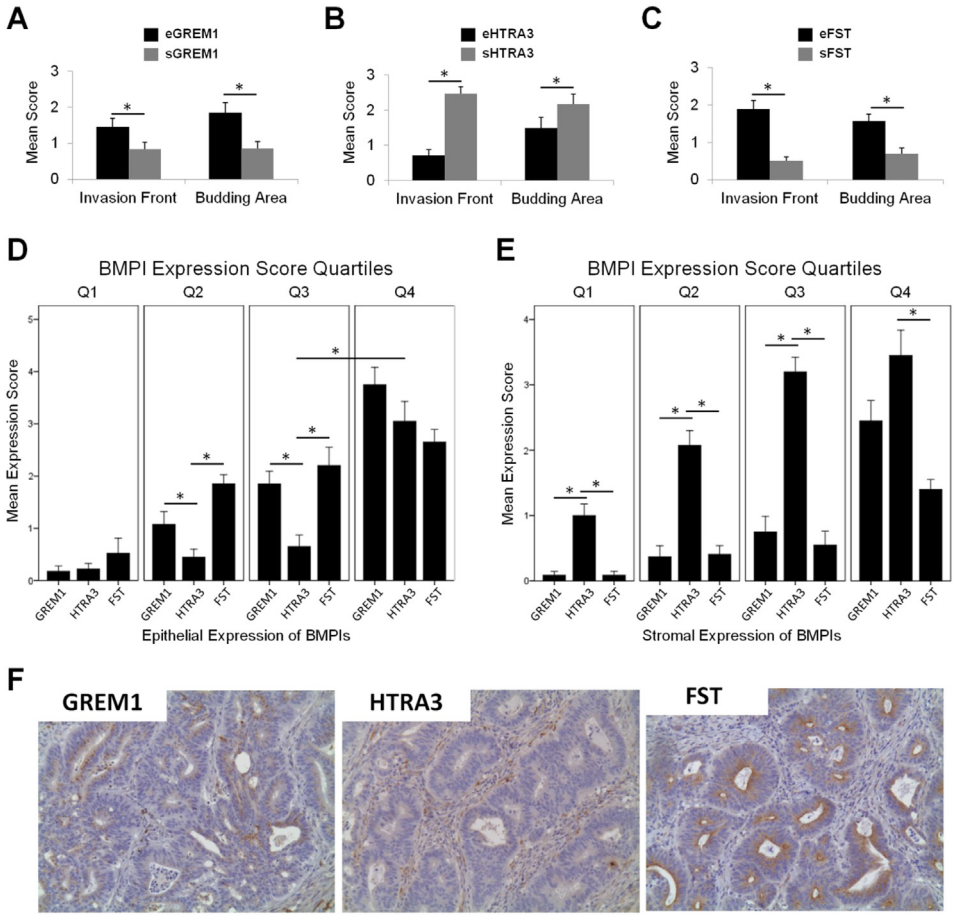

Figure 3 – Microenvironmental polarity of BMPI expression in colorectal cancer desmoplastic invasion fronts. (A–C) Mean expression scores of individual BMPI determinants in tumor-budding and tumor-budding-free invasion fronts. Asterisks demonstrate statistically significant differences with Wilcoxon test ($p < 0.05$). (D–E) Mean expression scores of individual BMPI determinants across Q1–Q4 quartiles. Asterisks demonstrate statistically significant differences with either Wilcoxon test (matched areas; $p < 0.05$) or Mann–Whitney *U*-test (non-matched areas; $p < 0.05$). (F) IHC snapshots from one selected area demonstrating the preferential expression of HTRA3 in cancer-associated fibroblasts (CAFs) and the parallel expression of GREM1 and FST in cancer cells. GREM1 signal is the lowest in this particular area, but is focally present in multiple neoplastic glands. Magnifications ×200.

whereby eHTRA3 almost reached the same expression levels with eGREM1 and eFST ($p > 0.05$; Wilcoxon test) (Figure 3D). This occurred due to a significant increase of eHTRA3 mean expression score between Q3 and Q4 areas ($p < 0.05$; Mann–Whitney *U*-test) (Figure 3D). On the other hand, sHTRA3 demonstrated a significantly higher mean expression score compared to either sGREM1 or sHTRA3 determinants ($p < 0.05$; Wilcoxon test), across increasing BMPI-expression score quartiles, without any exceptions (Figure 3E).

A representative area (tGREM1 = 2; tHTRA3 = 2; tFST = 6; tBMPI = 10) was selected to illustrate the microenvironmental polarity of BMPI expression. Immunoreactivity of HTRA3 was solely detected in the stromal compartment (sHTRA3 = 2; eHTRA3 = 0), while immunoreactivity of GREM1 and FST was detected in the epithelial compartment (sGREM1 = 0; eGREM1 = 2; sFST = 0; eFST = 6) of the tumor (Figure 3F).

These data briefly indicate that: (a) The major determinant of stromal BMP antagonism in CRC desmoplastic invasion fronts is HTRA3, and (b) The major determinants of epithelial BMP antagonism in CRC desmoplastic invasion fronts are GREM1 and FST. Collectively, these conclusions are reminiscent of the regulation of BMP antagonism in the desmoplastic invasion front through microenvironmental polarity.

3.4. *Epithelial expression of BMP inhibitor HTRA3 is differentially regulated between tumor-budding-bearing and tumor-budding-free desmoplastic invasion fronts*

Three diverse lines of evidence suggested that epithelial expression of HTRA3 followed a different pattern from the rest of the BMPIs that demonstrated a more conserved expression signature in CRC desmoplastic invasion fronts: First, eHTRA3 mean expression score shifted the pattern of the BMPI expression signature in the Q4 areas, by incorporating itself in one of the observed 'peaks' (Figure 1; red arrow). Second, this change was associated with significant increase in eHTRA3 levels of Q4 areas, when compared to the rest of the quartiles (Figure 3D). Third, eHTRA3 failed to correlate with two other BMPI determinants (sHTRA3, Spearman's rho = 0.187, $p > 0.05$; eFST, Spearman's rho = 0.196, $p > 0.05$)

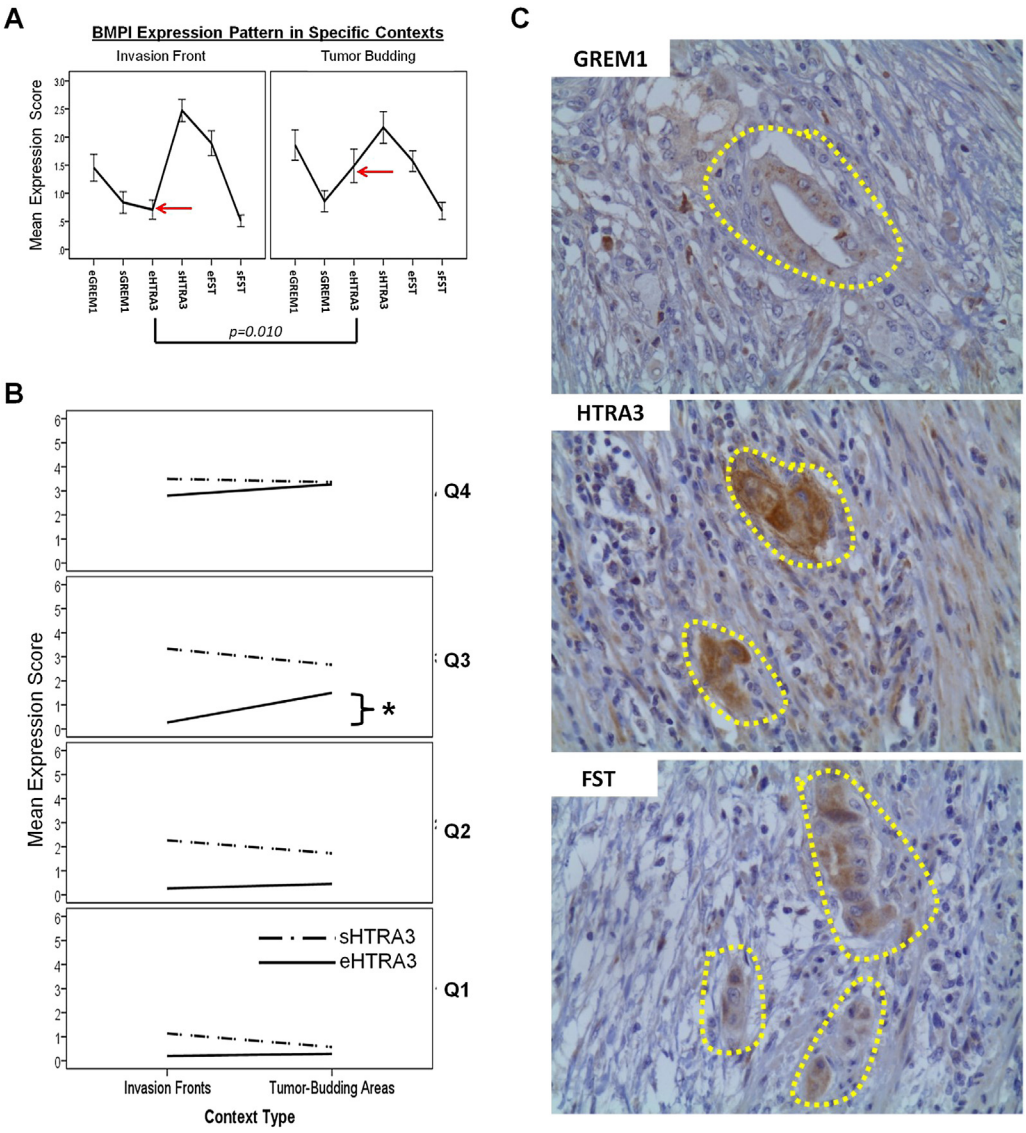

Figure 4 – Epithelial expression of BMP inhibitor HTRA3 is differentially regulated between tumor-budding and tumor-budding-free desmoplastic invasion fronts. (A) Patterns of mean expression scores of BMPI determinants between tumor-budding-bearing and tumor-budding-free areas. Red arrow; monitoring of the eHTRA3 determinant. Statistically significant differences demonstrated with Mann–Whitney *U*-test ($p < 0.05$). (B) Microenvironment polarity diagrams. Asterisk demonstrates statistically significant increase in the angle of inclination of eHTRA3 determinant in the Q3 quartile with a chi-square test ($p < 0.05$). (C) IHC snapshots from one area demonstrating strong immunoreactivity of HTRA3 in tumor budding. Dashed lines: tumor buds. Magnifications ×400.

(Figure 2C). These discrepancies allowed us to hypothesize that the microenvironmental polarity of HTRA3 is prone to disruption in elevated levels of BMP antagonism and could be possibly related to biological phenomena in the desmoplastic invasion front, with most appealing hypothesis that of tumor-budding regulation.

On this basis, we compared the mean expression scores of all six BMPI determinants between areas designated as "invasion fronts" and those designated as "tumor-budding areas", and found statistically significant increase of eHTRA3 expression levels ($p = 0.01$; Mann–Whitney *U*-test) in the latter areas (Figure 4A). The observed shift in HTRA3 expression pattern occurred in the Q3 quartile, as demonstrated from the microenvironmental polarity diagrams, where the angle of inclination was significantly different from "0" ($p < 0.05$; chi-square test) (Figure 4B). Notably, the co-assessment of Figures 3D and 4B revealed that the shift of HTRA3 microenvironmental polarity in Q3 quartile is followed by and may potentially justify the increased eHTRA3 expression observed in elevated BMP antagonism (Q4 quartile).

A selected area (tGREM1 = 2, tHTRA3 = 10, tFST = 3, tBMPI = 15) demonstrating significantly increased HTRA3 immunoreactivity in tumor-budding cells (eHTRA3 = 6; sHTRA3 = 4) is shown in Figure 4C. Although increased eHTRA3 expression was associated with occurrence of tumor budding (Figure 4A), we failed to demonstrate significant association with tumor budding grade ($p = 0.63$; Mann–Whitney *U*-test) (Supplementary Figure 5).

3.5. *Epithelial expression of BMP inhibitor HTRA3 holds pre-invasive information for tumor budding formation in desmoplastic invasion fronts*

Since tumor-budding is considered as an endpoint of cancer cell detachment from the proximal tumor invasion fronts, we sought to investigate whether eHTRA3 expression held any pre-invasive information for regulating it. An *a priori* goodness-of-fit test was performed and data were considered to be well-calibrated ($p = 0.339$; Hosmer–Lemeshow test) for logistic regression analysis. The analysis demonstrated a statistically significant relationship between eHTRA3 expression score and tumor-budding presence ($p = 0.025$). ROC curves were conducted to evaluate the effectiveness of eHTRA3 in differentiating between tumor-budding-bearing and tumor-budding-free desmoplastic invasion fronts. The area under the curve (AUC) was 0.645 (Figure 5A) with a sensitivity of 89.1% and specificity of 20%, as depicted through the classification table, showing that eHTRA3 is sensitive but not specific.

We exploited the possibility that BMP antagonism could influence the potential of eHTRA3 in discriminating tumor-budding-free from tumor-budding-bearing microenvironments. By repeating logistic regression for Q1–Q4 quartiles independently (subgroup analysis), we found statistically significant relationship between eHTRA3 expression score and tumor-budding-free microenvironment ($p = 0.04$) in the Q3 quartile (Figure 5B). Associations in other quartiles were non-significant (Figure 5B). The AUC for Q3 was 0.767 with 100% sensitivity and 50% specificity, indicating that eHTRA3 becomes more sensitive and specific when measured in areas with certain degree of BMP antagonism (i.e. tBMPI = 8–11).

As a proof-of-concept, we demonstrated that high-levels of eHTRA3 were expressed in poorly-differentiated cancer cell cohorts positioned in the invasive margins (Figure 5C yellow dotted line) in close proximity to the desmoplastic stroma. A striking difference of eHTRA3 expression between this cancer cell subpopulation (Figure 5C; yellow arrows) and the tumor core cells (Figure 5C; yellow asterisks) has been illustrated in many cases implying that these cells could probably demonstrate an "early tumor-budding phenotype". Morphologically, these cells retained some level of cell-to-cell adhesion with the proximal invasion fronts (Figure 5C).

3.6. *Validation experiments in an independent patient cohort*

Significant difference ($p < 0.05$, Mann–Whitney *U*-test) of eHTRA3 expression between tumor budding-bearing and -free microenvironments was demonstrated in an independent cohort of 38 patients with CRC (Figure 6A). Expression scores from multiple areas of the same case were combined in one mean HTRA3 expression score per case and correlation with tumor budding was, then, examined. The expression level of eHTRA3 was significantly increased ($p = 0.019$,

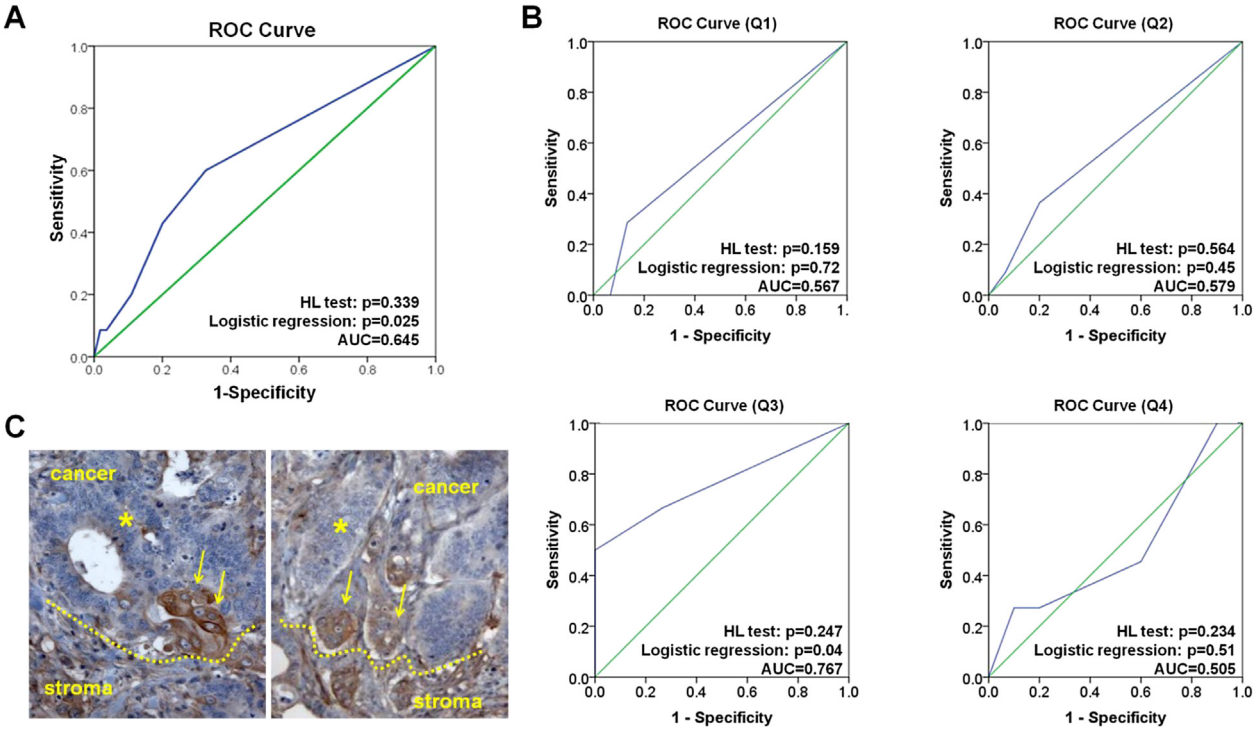

Figure 5 – Epithelial expression of BMP inhibitor HTRA3 holds pre-invasive information for tumor budding formation in colorectal cancer desmoplastic invasion fronts. (A–B) ROC curves demonstrating the potential of the eHTRA3 expression levels in predicting a tumor-budding-free desmoplastic microenvironment in the entire population of areas (A) or in specific levels of BMP antagonism (B). Area under the curve (AUC), *p*-values from logistic regression model and results from the Hosmer–Lemeshow (HL) test are described for each curve independently. (C) IHC of HTRA3 in two areas, demonstrating high eHTRA3 expression in cancer cells lining the invasion front, predicting their potential for forming buds. Asterisks: negative tumor-core cells; dashed lines: tumor-host cell interface; arrows: HTRA3-positive cancer cell subpopulations of the invasion front undergoing detachment and possible early tumor budding formation. Magnifications ×250.

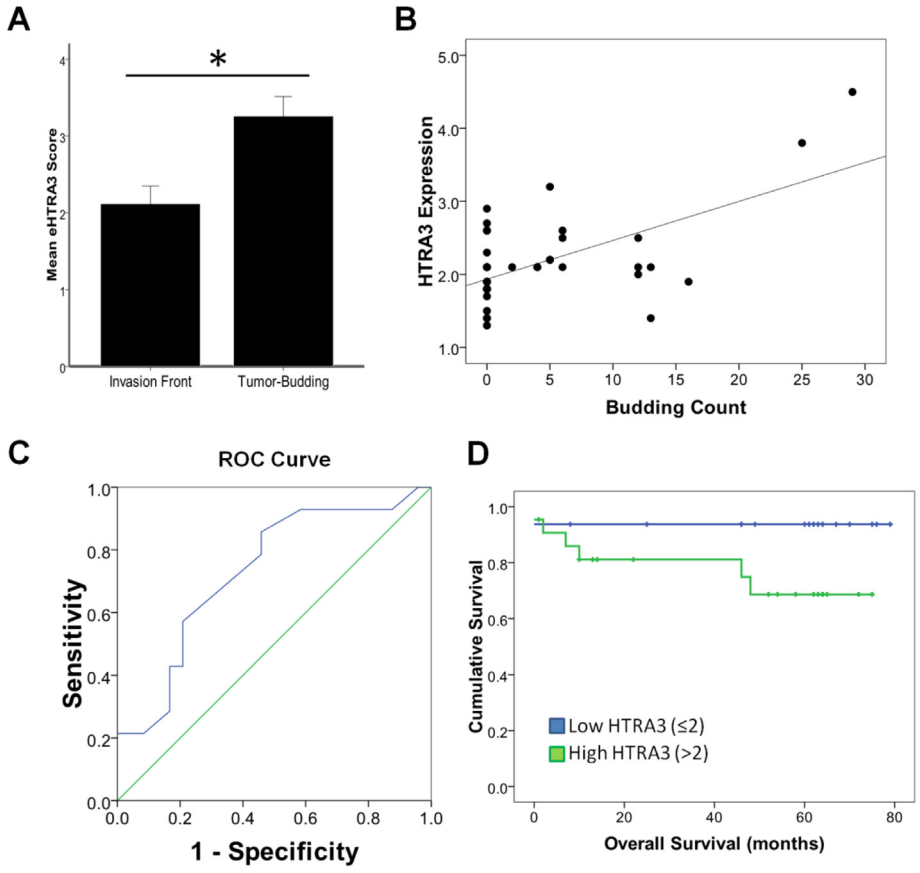

Figure 6 – (A) Mean expression score of epithelial HTRA3 between tumor-budding-bearing and tumor-budding-free areas in the validation cohort. Statistically significant difference demonstrated with Mann–Whitney *U*-test ($p < 0.05$). (B) Correlation between tumor budding score and mean eHTRA3 expression level in each of the 38 cases of the validation cohort. (C) ROC curve in the validation cohort. Area under the curve (AUC), *p*-values from logistic regression model and results from the Hosmer–Lemeshow (HL) test are shown. (D) Kaplan–Meier overall survival of the 38 patients of the validation cohort, stratified according to the cut-off level of eHTRA3 expression score 2. Note that high eHTRA3 expression is an independent predictor of poor survival.

spearman's rho = 0.349), following an increase in the tumor-budding score at the level of the invasion front (Figure 6B). Logistic regression was conducted in the validation cohort, by additionally taking into consideration patient demographic data [gender, T-category, Crohn's like reaction and tumor-infiltrating lymphocytes (marked TILs)], as shown in Supplementary Table 1. Interestingly, the expression of HTRA3 in cancer cells lining the invasion front could still significantly ($p = 0.042$, AUC = 0.731) predict the presence of tumor budding-free areas with 64% sensitivity and 95% specificity (Figure 6C).

It has been previously denoted that tumor-budding is an independent factor of poor prognosis in CRC (Barresi et al., 2012; Mitrovic et al., 2012; Wang et al., 2009), an observation that was also confirmed in this 38-patient cohort (Supplementary Figure 6). Therefore, since eHTRA3 expression was associated with tumor budding, as depicted through our collective observations, we hypothesized that it could also be related to patient survival. Indeed, survival analysis using Kaplan–Meier plots demonstrated that ~50% of CRC patients with highest expression of eHTRA3 (i.e. with a score of >2) had poorer prognosis than that of the remainder 50% with the lowest expression (Figure 6D).

4. Discussion

Emerging technologies, such as mass spectrometry-based proteomics and integrative bioinformatics (Karagiannis et al., 2010), allowed us to initially propose the coordinated deregulation of multiple determinants of BMP antagonism in colorectal cancer (Karagiannis et al., 2012a, 2013a). The current study has successfully validated these observations and illustrated a more solid perspective on the individual contribution of each one of the BMPI determinants in CRC desmoplastic invasion fronts. Interestingly, we noted a synchronous and coordinated expression of GREM1, FST and HTRA3 in both stromal and epithelial compartments of desmoplastic cancers, which followed a consistent pattern as the levels of BMP antagonism elevated. This observation fits well into our previously described model of "multilayered BMP antagonism hypothesis" (Karagiannis et al., 2013a), stating that CRC cells of the advanced invasion front can only flourish in a microenvironment devoid of the tumor-suppressive properties of the BMP signaling: To guarantee its absolute disruption, the cancer cells deploy multiple "layers" of BMP antagonism, including the genetic level (i.e. SMAD4/

BMPR2 functional mutations) (Kodach et al., 2008; Kotzsch et al., 2008), the epigenetic level (i.e. methylation of BMP2 gene promoter) (Wen et al., 2006), as well as the proteomic level (i.e. antagonistic regulation of BMP ligands by paracrine production of BMP antagonists) (Sneddon et al., 2006). Here, we demonstrated that multiple BMPIs could be determinants of this multilayered BMP inhibition process.

By investigating the BMPI signature pattern in desmoplastic areas, we observed the presence of "microenvironmental polarity" in the expression levels of three individual BMPIs. In particular, FST and GREM1 demonstrated preferential expression in the epithelial compartment of the tumors, while HTRA3 in the stromal compartment. However, a significant shift in the epithelial expression of HTRA3 was noticed with increasing levels of overall BMP antagonism as well as with tumor-budding areas. On this basis, we concluded that the level of epithelial expression of HTRA3 is the rate-limiting step for maintenance of a tumor-budding-free microenvironment in CRC. The logistic regression model and the respective ROC curves suggested that as long as the expression of the BMP antagonist HTRA3 is low in cancer cells lining the invasion front, there is a ~90% chance that the cancer will harbor a tumor-budding-free desmoplastic microenvironment. Only after the microenvironmental polarity of HTRA3 expression towards the stroma is disrupted (i.e. the eHTRA3 and sHTRA3 determinants obtain expression scores without significant differences), the possibility of tumor-budding formation is significantly enhanced. However, to which extent the HTRA3-dependent BMP antagonism is simply phenotypically coincidental or causatively linked with the process of tumor budding formation remains to be elucidated.

Although we observed significant predictive power of HTRA3 expression in identifying tumor budding-free microenvironments, this marker did not present with astounding sensitivity in defining the process. We believe that this was quite an expected and reasonable outcome, especially since tumor-budding formation is a rather complicated process, possibly mediated by multiple EMT-regulating pathways (Mitrovic et al., 2012; Zlobec and Lugli, 2011, 2009), besides BMP. Interestingly though, our logistic regression model represents a very delicate means of showing that only a specific portion of CRC patients that eventually develop enhanced BMP antagonism (through aberrant HTRA3 secretion) will eventually form tumor buds in the invasion front. A better definition of this CRC patient subgroup, along with a mechanistic explanation as to how and why HTRA3 microenvironmental polarity is shifted in those, should be further explored in the future.

Interestingly, tumor-budding has been clearly associated to malignant phenomena, such as epithelial-to-mesenchymal transition (EMT) (Zlobec and Lugli, 2011). Also, it has been suggested as an independent and reproducible factor of poor prognosis in CRC and other types of cancer, capable of stratifying those into risk groups, in a more meaningful fashion than the traditional TNM system (Barresi et al., 2012; Karamitopoulou et al., 2012; Mitrovic et al., 2012; Wang et al., 2009). However, the assessment of the degree of tumor-budding is highly prone to laboratory- and observer-based biases. Therefore, well-standardized histological and immunohistochemical criteria for tumor budding evaluation remain to be determined in the future (Mitrovic et al., 2012). As such, the prognostic potential of HTRA3 as a predictive immunomarker, in the area of tumor-budding occurrence should not be disregarded. The epithelial expression of HTRA3 or other relevant markers could be used for accurate measurement of this biological process in CRC, if they prove to be sensitive and specific in large patient cohorts.

An important feature is the utilization of an independent patient cohort for verifying the predictive potential of HTRA3 in discriminating between tumor-budding-free and -bearing microenvironments. By repeating logistic regression in the validation cohort, it should be noted that potential confounding factors were taken into consideration and the classification model was properly corrected. As such, we are relatively confident that HTRA3 alone possesses a strong potential to be implicated with tumor budding in a mechanistic aspect. However, important molecular aspects of CRC, such as microsatellite stability status, should not be underestimated, as they could also be related to the mechanism and nature of tumor invasion. It is known that MSI CRC presents with lower aggressiveness (Buckowitz et al., 2005) that may also be reflected in the macroscopic appearance of tumor configuration (Sasaki et al., 1998). This is also supported by the fact that MSI tumors lose the EMT-promoting properties of TGF-beta signaling through mutational inactivation of TGFBR3 (Warusavitarne et al., 2009), and such impairment of EMT may have an impact on the progression of the disease (Pino et al., 2009). As such, the currently described BMP antagonists could theoretically complement or even replace the missing EMT-promoting role of the TGF-beta pathway in MSI patients to promote EMT and local invasion/tumor budding formation. This speculation remains to be explored in the future. Unfortunately, direct data on microsatellite status were not available in our patient cohorts in the current study. However, based on previous knowledge (Shia et al., 2003; Wright and Stewart, 2003), there is certain histopathology that is correlated with defects in mismatch repair mechanisms in colon cancers. In particular, Crohn's-like lymphoid reaction and marked tumor-infiltrating lymphocytes (marked TILs), have been associated and very well-correlated with microsatellite instability. Information on these histologies were fortunately available in our verification cohort (supplementary Table 1) and these data were used for correcting respective biases of the logistic regression model.

It should be noted that the determinants of the BMPI signature might regulate a diverse repertoire of biological responses in the desmoplastic invasion front. One of them, GREM1 is a highly-selective inhibitor of certain BMP ligands, in particular BMP2, -4 and -7 (Kosinski et al., 2007). However, GREM1 is also capable of binding to and activating phosphorylation of vascular endothelial growth factor receptor-2 (VEGFR2) in a BMP-independent fashion (Mitola et al., 2010), leading to the formation of VEGFR2/$\alpha_v\beta_3$-integrin complexes and angiogenesis promotion (Ravelli et al., 2012). Moreover, FST is less selective and although it heterodimerizes with BMPs with some affinity, the major pathway in the TGF-β superfamily of proteins that it regulates is the activin/inhibin pathway (Beites et al., 2009). Finally, HTRA3 is an extracellular protease that remodels ECM in a manner that sequesters members of

the TGF-β superfamily, reducing their bioavailability (Tocharus et al., 2004). Consequently, the observed BMPI signature will not necessarily exert a tumor-regulatory effect (if indeed has any), exclusively through BMP antagonism, since these pleiotropic effects of the aforementioned BMPIs are well-documented.

In conclusion, three major characteristics jointly described the BMPI expression signature: First, the synchronous and coordinated stromal and epithelial expression of individual BMPIs in desmoplastic areas, which demonstrated that all three of them contribute to increasing levels of BMP antagonism. Second, the presence of microenvironmental polarity in the BMPI pattern of expression, which was indicated through the preferential expression of HTRA3 in the stromal, and a parallel FST/GREM1 expression in the epithelial component of the investigated areas. Third, the expression of HTRA3 in the epithelial compartment of the tumors demonstrated a significant predictive power to discriminate between tumor-budding-bearing and tumor-budding-free desmoplastic microenvironments. Together, these findings form the basis for understanding signaling dynamics of BMP antagonism in CRC desmoplastic invasion front and shed some insight in the regulation of the core pathway.

Acknowledgments

George S. Karagiannis is supported by University Health Network and Mount Sinai Hospital, Toronto, ON, Canada. The authors would like to thank Kuruzar Gordana for technical assistance.

Author contributions

Conceptualized study: GSK; Designed, performed, and interpreted IHC: GSK, AT, DM, AG, RK and RHR; Performed statistical analyses: GSK; Prepared IHC figures: AT; Wrote manuscript: GSK; Revised manuscript: GSK, AT, DM, AG, RK, RHR, EPD.

Appendix A. Supplementary data

Supplementary data related to this article can be found at http://dx.doi.org/10.1016/j.molonc.2014.04.004.

REFERENCES

Alarmo, E.L., Kallioniemi, A., 2010. A bone morphogenetic proteins in breast cancer: dual role in tumourigenesis? Endocr. Relat. Cancer 17, R123–R139.

Altman, D.G., McShane, L.M., Sauerbrei, W., Taube, S.E., 2012. Reporting recommendations for tumor marker prognostic studies (REMARK): explanation and elaboration. PLoS Med. 9, e1001216.

Barresi, V., Reggiani Bonetti, L., Branca, G., Di Gregorio, C., Ponz de Leon, M., Tuccari, G., 2012. Colorectal carcinoma grading by quantifying poorly differentiated cell clusters is more reproducible and provides more robust prognostic information than conventional grading. Virchows Arch. 461, 621–628.

Beck, S.E., Jung, B.H., Fiorino, A., Gomez, J., Rosario, E.D., Cabrera, B.L., et al., 2006. Bone morphogenetic protein signaling and growth suppression in colon cancer. Am. J. Physiol. Gastrointest. Liver Physiol. 291, G135–G145.

Beites, C.L., Hollenbeck, P.L., Kim, J., Lovell-Badge, R., Lander, A.D., Calof, A.L., 2009. Follistatin modulates a BMP autoregulatory loop to control the size and patterning of sensory domains in the developing tongue. Development 136, 2187–2197.

Bissell, M.J., Radisky, D., 2001. Putting tumours in context. Nat. Rev. Cancer 1, 46–54.

Buckowitz, A., Knaebel, H.P., Benner, A., Blaker, H., Gebert, J., Kienle, P., et al., 2005. Microsatellite instability in colorectal cancer is associated with local lymphocyte infiltration and low frequency of distant metastases. Br. J. Cancer 92, 1746–1753.

Grin, A., Messenger, D.E., Cook, M., O'Connor, B.I., Hafezi, S., El-Zimaity, H., et al., 2013. Peritoneal elastic lamina invasion: limitations in its use as a prognostic marker in stage II colorectal cancer. Hum. Pathol. 44, 2696–2705.

Karagiannis, G.S., Berk, A., Dimitromanolakis, A., Diamandis, E.P., 2013a. Enrichment map profiling of the cancer invasion front suggests regulation of colorectal cancer progression by the bone morphogenetic protein antagonist, gremlin-1. Mol. Oncol. 7, 826–839.

Karagiannis, G.S., Pavlou, M.P., Diamandis, E.P., 2010. Cancer secretomics reveal pathophysiological pathways in cancer molecular oncology. Mol. Oncol. 4, 496–510.

Karagiannis, G.S., Petraki, C., Prassas, I., Saraon, P., Musrap, N., Dimitromanolakis, A., et al., 2012a. Proteomic signatures of the desmoplastic invasion front reveal collagen type XII as a marker of myofibroblastic differentiation during colorectal cancer metastasis. Oncotarget 3, 267–285.

Karagiannis, G.S., Poutahidis, T., Erdman, S.E., Kirsch, R., Riddell, R.H., Diamandis, E.P., 2012b. Cancer-associated fibroblasts drive the progression of metastasis through both paracrine and mechanical pressure on cancer tissue. Mol. Cancer Res. 10, 1403–1418.

Karagiannis, G.S., Schaeffer, D.F., Cho, C.K., Musrap, N., Saraon, P., Batruch, I., et al., 2014. Collective migration of cancer-associated fibroblasts is enhanced by overexpression of tight junction-associated proteins claudin-11 and occludin. Mol. Oncol. 8, 178–195.

Karamitopoulou, E., Zlobec, I., Born, D., Kondi-Pafiti, A., Lykoudis, P., Mellou, A., et al., 2012. Tumour budding is a strong and independent prognostic factor in pancreatic cancer. Eur. J. Cancer 49, 1032–1039.

Kodach, L.L., Bleuming, S.A., Musler, A.R., Peppelenbosch, M.P., Hommes, D.W., van den Brink, G.R., et al., 2008. The bone morphogenetic protein pathway is active in human colon adenomas and inactivated in colorectal cancer. Cancer 112, 300–306.

Kosinski, C., Li, V.S., Chan, A.S., Zhang, J., Ho, C., Tsui, W.Y., et al., 2007. Gene expression patterns of human colon tops and basal crypts and BMP antagonists as intestinal stem cell niche factors. Proc. Natl. Acad. Sci. U S A 104, 15418–15423.

Kotzsch, A., Nickel, J., Seher, A., Heinecke, K., van Geersdaele, L., Herrmann, T., et al., 2008. Structure analysis of bone morphogenetic protein-2 type I receptor complexes reveals a mechanism of receptor inactivation in juvenile polyposis syndrome. J. Biol. Chem. 283, 5876–5887.

Mitola, S., Ravelli, C., Moroni, E., Salvi, V., Leali, D., Ballmer-Hofer, K., et al., 2010. Gremlin is a novel agonist of the major proangiogenic receptor VEGFR2. Blood 116, 3677–3680.

Mitrovic, B., Schaeffer, D.F., Riddell, R.H., Kirsch, R., 2012. Tumor budding in colorectal carcinoma: time to take notice. Mod. Pathol. 25, 1315–1325.

Namkoong, H., Shin, S.M., Kim, H.K., Ha, S.A., Cho, G.W., Hur, S.Y., et al., 2006. The bone morphogenetic protein antagonist gremlin 1 is overexpressed in human cancers and interacts with YWHAH protein. BMC Cancer 6, 74.

Pino, M.S., Kikuchi, H., Zeng, M., Herraiz, M.T., Sperduti, I., Berger, D., et al., 2009. Epithelial to mesenchymal transition is impaired in colon cancer cells with microsatellite instability. Gastroenterology 138, 1406–1417.

Ravelli, C., Mitola, S., Corsini, M., Presta, M., 2012. Involvement of alphavbeta3 integrin in gremlin-induced angiogenesis. Angiogenesis 16, 235–243.

Reddi, A.H., Reddi, A., 2009. Bone morphogenetic proteins (BMPs): from morphogens to metabologens. Cytokine Growth Factor Rev. 20, 341–342.

Saaf, A.M., Halbleib, J.M., Chen, X., Yuen, S.T., Leung, S.Y., Nelson, W.J., et al., 2007. Parallels between global transcriptional programs of polarizing Caco-2 intestinal epithelial cells in vitro and gene expression programs in normal colon and colon cancer. Mol. Biol. Cell 18, 4245–4260.

Sasaki, S., Masaki, T., Umetani, N., Shinozaki, M., Yokoyama, T., Ono, M., et al., 1998. Microsatellite instability is associated with the macroscopic configuration of neoplasms in patients with multiple colorectal adenomas. Jpn. J. Clin. Oncol. 28, 427–430.

Shia, J., Ellis, N.A., Paty, P.B., Nash, G.M., Qin, J., Offit, K., et al., 2003. Value of histopathology in predicting microsatellite instability in hereditary nonpolyposis colorectal cancer and sporadic colorectal cancer. Am. J. Surg. Pathol. 27, 1407–1417.

Singh, A., Morris, R.J., 2010. The Yin and Yang of bone morphogenetic proteins in cancer. Cytokine Growth Factor Rev. 21, 299–313.

Sneddon, J.B., 2009. The contribution of niche-derived factors to the regulation of cancer cells. Methods Mol. Biol. 568, 217–232.

Sneddon, J.B., Zhen, H.H., Montgomery, K., van de Rijn, M., Tward, A.D., West, R., et al., 2006. Bone morphogenetic protein antagonist gremlin 1 is widely expressed by cancer-associated stromal cells and can promote tumor cell proliferation. Proc. Natl. Acad. Sci. U S A 103, 14842–14847.

Tocharus, J., Tsuchiya, A., Kajikawa, M., Ueta, Y., Oka, C., Kawaichi, M., 2004. Developmentally regulated expression of mouse HtrA3 and its role as an inhibitor of TGF-beta signaling. Dev. Growth Differ 46, 257–274.

Wang, L.M., Kevans, D., Mulcahy, H., O'Sullivan, J., Fennelly, D., Hyland, J., et al., 2009. Tumor budding is a strong and reproducible prognostic marker in T3N0 colorectal cancer. Am. J. Surg. Pathol. 33, 134–141.

Warusavitarne, J., McDougall, F., de Silva, K., Barnetson, R., Messina, M., Robinson, B.G., et al., 2009. Restoring TGFbeta function in microsatellite unstable (MSI-H) colorectal cancer reduces tumourigenicity but increases metastasis formation. Int. J. Colorectal Dis. 24, 139–144.

Wen, X.Z., Akiyama, Y., Baylin, S.B., Yuasa, Y., 2006. Frequent epigenetic silencing of the bone morphogenetic protein 2 gene through methylation in gastric carcinomas. Oncogene 25, 2666–2673.

Wright, C.L., Stewart, I.D., 2003. Histopathology and mismatch repair status of 458 consecutive colorectal carcinomas. Am. J. Surg. Pathol. 27, 1393–1406.

Zeisberg, M., Hanai, J., Sugimoto, H., Mammoto, T., Charytan, D., Strutz, F., et al., 2003. BMP-7 counteracts TGF-beta1-induced epithelial-to-mesenchymal transition and reverses chronic renal injury. Nat. Med. 9, 964–968.

Zlobec, I., Lugli, A., 2011. Epithelial mesenchymal transition and tumor budding in aggressive colorectal cancer: tumor budding as oncotarget. Oncotarget 1, 651–661.

Zlobec, I., Lugli, A., 2009. Invasive front of colorectal cancer: dynamic interface of pro-/anti-tumor factors. World J. Gastroenterol. 15, 5898–5906.